NOVEL PASSIVE AND ACTIVE FLOW CONTROL FOR HIGH LIFT

L.L.M. Veldhuis* , D.P. Jansen* , J. El Haddar* , G. Correale*
*Delft University of Technology

Keywords: *High Lift, Flow Control*

Abstract

In this paper we discuss the separation control capabilities of various passive and active techniques. The goal of this research is to further quantify the possibilities of enhanced high lift systems for a multi-element wing that consists of a main wing plus fowler flap. To study the effect of the control techniques, experimental investigations where performed in different low speed windtunnels on a single element airfoil and wing-flap model. The results show that a lift enhancement of 18% can be obtained on single element airfoils using nano-pulsed plasma actuators. An attempt was made to enhance the high lift performance on a wing flap model through increased flap deflection combined with separation control by applying several passive and active techniques on the flap leading edge. It was shown that the application of a circular cylinder in front of the flap leads to a noticeable increase in the lift coefficient in cases where the flap boundary layer tends to exhibit trailing edge stall. The other applied control techniques had a limited effect which was either due to limited momentum input or the occurrence of wake bursting.

1 Introduction

Over the past decades several innovative techniques to control flow separation over airfoils have been proposed. In recent years especially the research on active flow control methods has received interest. The application of active blowing, suction and the utilization of zero mass transfer synthetic jets (SJA) [1, 2, 3, 4] have shown to be capable of postponing the separation to some extend. However, the practical implementation of these active methods, in general, leads to an unwanted increase in mass, degradation of the wing's structural integrity (SJA) and increased power demands to drive pumps (suction or blowing) or excite piezo-electrical systems and associated hardware.

Although attractive from the point of further improvement opportunities, many active systems have not matured to be incorporated in modern transport aircraft currently developed. This is partly due to the need to adapt the wing or flap internal structure for most of these systems. In this respect it is attractive to revisit the possible passive control methods and compare them with active methods that require only a limited adaptation of the wings structure, enabling application of the particular technique as a retrofit.

At Delft University a research program is undertaken which aims at developing novel passive and active control techniques to enhance the high lift capabilities of wings. Especially the effect of modern techniques like plasma actuators is investigated. In this paper the experimental research on passive on and off-surface control elements as well as active techniques in the form of Nano-pulsed actuators will be addressed. The goal of this part of the project is to get further insight in the possibilities to employ extended (Fowler) flap deflection which under normal, uncontrolled, conditions would lead to serious flow separation over the flap surface. This separation is prevented by applying three different control techniques:

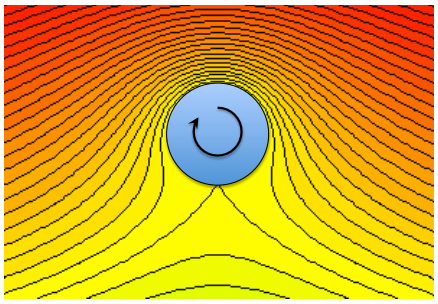

Fig. 1 Flow field around a circular cylinder with rotation. The circulation strength is chosen such that the 2 stagnation points coincide at the lower side.

plasma actuators, drooped spoiler and periodic flow excitation based on off-surface positioned cylinders.

2 Background on high lift enhancement

To better understand how the parameters determine the high lift and flow separation characteristics of the high lift system, it is necessary to accurately identify the interaction effects of multiple elements. A very good overview is given by Smith [9] and later by van Dam [10] and the reader is referred to these references for a complete overview of high lift aerodynamics in general. An interesting point that is related to the current research is question as to what maximum lift may be obtained.

When comparing the lifting capabilities of a system equipped with slat and flap (either single of multiple flaps) one may argue (see [9]) that the theoretical lift coefficient that can be obtained is the one that is found for inviscid flow over a circular cylinder airfoil with both stagnation points at the lower side (fig. 1). The lift coefficient is in this case

$$C_l = 4\pi$$

This is of course an extreme case which is far from the practical layout of a wing with high lift elements deployed. However, a circular arc airfoil may be quite close to the optimum flow field that is found for a real high lift model (fig. 2). In this case the flow is extremely curved and the (inviscid) theoretical maximum lift coefficient will

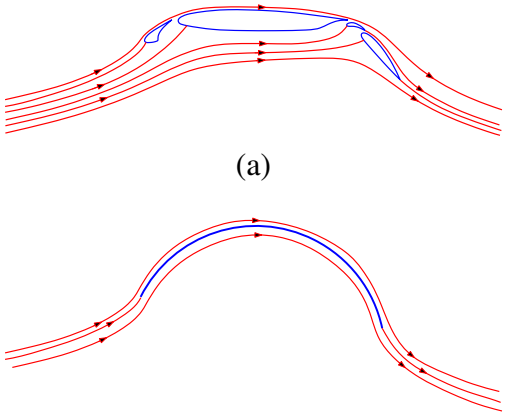

Fig. 2 Typical flow pattern over a three element high lift airfoil (a) and a circular arc airfoil (b) in inviscid flow. The streamline pattern shows close resemblance between the two.

be

$$C_{l_{max}} = 4\pi/\sqrt{2} \approx 8.8$$

Even this value is way beyond the typical values that are found for modern transport aircraft. In fact one of the main limitations for reaching values close to this inviscid value is the flow separation on either the main wing and/or the flap in real viscous flows. Hence, in case the maximum lift coefficient for a given layout is to be maximized the occurrence of flow separation needs to be minimized. If such an approach would be successful, the high lift system would benefit from very large flap deflections. In this research flap deflections angle larger than 40^o are discussed in conjunction with possible new passive and active flow control techniques. As the current CFD (RANS) approaches have difficulty in accurately predicting flow with severe separation, this research is performed through windtunnel experiments.

3 Experimental setup and test approach

3.1 Windtunnel and models

3.1.1 Windtunnels

Experimental investigations were performed in a 2 different low speed windtunnels: the M/W-tunnel (Model 1) and the Low Turbulence Tun-

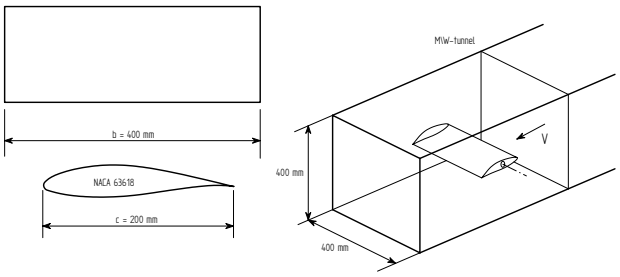

Fig. 3 Model 1: Straight NACA 63618 wing model dimensions and geometry.

nel (LTT) (Model 2). Both windtunnels are located in the Aerodynamics Laboratory of the Faculty of Aerospace Engineering of Delft University of Technology. The M/W-tunnel consists of an open circuit which produces a rectangular jet of $400 \times 400mm$. The turbulence level in this windtunnel is typically in the order of 0.1%.

The LTT is closed circuit windtunnel with an octagonal test section of $1.80m \times 1.20m$. The maximum speed in this facility is $V_{max} = 120m/s$, while the turbulence level is very low, in the order of $0.01\% - 0.2\%$. The pressure recording in this facility is done with a 200 port electronic transducer (PSI-DMT, "Initium system"). Boundary layer transition is recorded with an electronically amplified stethoscope. Furthermore, wake and boundary layer velocity profiles were measured with a dedicated BL-probe.

3.1.2 Model 1, Single element airfoil

The first wing model that was investigated is based on a span of $b = 400mm$ and constant chord of $c = 150mm$ having a *NACA-63618* airfoil (fig. 3). The model is positioned between walls to obtain 2-dimensional flow. This setup was chosen to check the effect of Nano-pulsed actuator control [23] of leading edge separation at different wind speeds (Reynolds numbers) in a range that can not be attained with standard Di-electric barrier discharge (DBD) actuators [22, 15]. The main aerodynamic coefficients (lift, drag and pitching moment) were measured with an external 6-component balance.

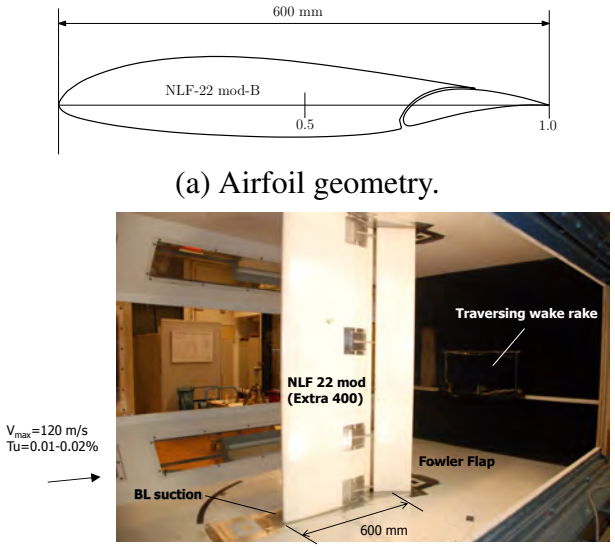

(a) Airfoil geometry.

(b) Wing flap model (Model 2) in Low Speed windtunnel.

Fig. 4 Model 2: NLF-22-mod-B wing model with extendable flap (X400).

3.1.3 Model 2, Multi-element airfoil

The second model that was investigated consists of wing-flap model mounted vertically and spanning the windtunnel over the full height (fig. 4). This modified NLF22 airfoil is in fact used on the Extra-400 aircraft[1]. It was used in an earlier test campaign in which the flap overlap and gap were optimized[7]. The flap could be deflected over a range from $\delta_f = 0^o$ to 60^o to produce either attached, partly separated or fully separated flow over the flap upper surface. Especially the larger flap deflections are investigated with respect to the control capabilities of passive and active techniques. The basic characteristics were obtained through surface pressure and wake rake measurements. To prevent unwanted flow separation on the windtunnel upper and lower wall (wall-model juncture) the boundary layer was removed through suction holes connected to a high capacity pump.

3.2 Flow control devices

[1] German built 6 seater, all composite turboprop aircraft

3.2.1 Plasma Generators

Standard DBD actuators The potential of plasma actuators for flow control has been recognized by a number of researchers [17, 18, 19, 21, 22, 14, 15, 13, 12]. Most of the existing work has focused on the development of standard dielectric barrier discharge (SDBD) actuators. Their working principle is based on applying a high voltage (5-30 kV) signal to two staggered electrodes separated by dielectric material in order to create a biased flow of ions and electrons which adds momentum to the main flow (see fig. 5a). Using this technique, near-wall jets on the order of 1-2 mm thick have been created, with jet speeds approaching 8m/s. These have been used to successfully control low-speed separated flows The effectiveness of SDBD actuators has been found to be sensitive to a number of parameters. It has shown that relatively thick dielectrics tend to produce larger changes in momentum, while Enlo et al [16] have shown that when using non-conventional thin wire electrodes, decreasing the wire diameter increases the change of momentum at a given input power. The form of the input signal has also been shown to be significant. More recently Kotsonis [17] has shown that much larger changes in momentum can be obtained using combinations of sinusoidal excitation and signals with steep rises and falls.

However, one of the limitations of SDBD actuators is their rather low momentum input which makes them suited for low Reynolds number flows only [12]. Typical Reynolds numbers at which a beneficial separation suppressing effect was found are in the range $Re = 20,000 - 50,000$, which is too low for general applications on aircraft.

Nano-pulsed actuators Over the last three years a new class of plasma flow actuators has been developed which work on a completely different principle [23]. These so-called nano-pulse dielectric barrier discharge (NPDBD) actuators have geometries similar their SDBD counterparts, but use a high-energy (20-50 mJ) short-duration (10-100 nsec) pulses to produce localized heating in the order of $200 - 300K$ (fig, 5b). This process delivers very little direct momentum input, but generates shock waves which radiate from the actuator that interact with the outer flow [24, 20]. Recent experiments carried out by the TUD Aerodynamics group have demonstrated that NPDBD actuators can be used to reattach airfoil flows with leading-edge separation, leading to increases in maximum lift of up to 20% at wind speeds up to 40 m/s [20]. This may be the result of a number of mechanisms, including the periodic forcing of laminar-turbulent transition, shock-shear layer interactions, or the creation of large vortical structures. The latter have been observed in Schlieren imaging [20]. However, the parameters that influence the effectiveness of NPDBD separation control have yet to be fully explored. Furthermore, the basic mechanisms of the flow phenomena that occur is a point of continued research. Nevertheless, since beneficial results were obtained over a stalled NACA-63618 airfoil is decided to apply the NPDBD actuator on the flap of Model 2 as well.

3.2.2 Cylinder

In the selection of a flow control device the structural simplicity of application as well as the minimization of power usage is crucial. For this reason a novel passive technique was tried in which a cylinder is placed directly upstream of the flap leading edge of Model 2. The beneficial effect of such a device was already discussed by Veldhuis and van der Steen [6], who applied a likewise setup on a simplified flap model. The working principle of the device is based on the generation of von K*á*rm*á*n vortex street that performs two actions: a) the introduction of additional vorticity which enhances the mixing process in the boundary layer and b) the unsteady pulsing of the flow due to the periodic shedding of the vortices behind the cylinder (fig. 6b). The latter effect has been described also by Nishri et al [26] who found a beneficial effect of pulsed excitation of the flow.

Since the system is passive its structural layout is very simple and in a practical application

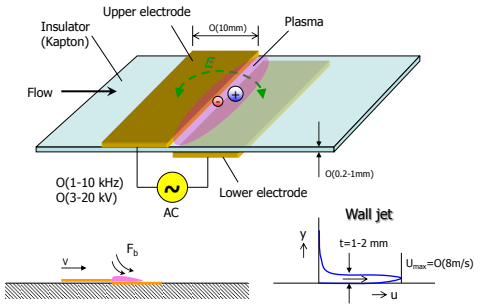

a) SDBD actuator

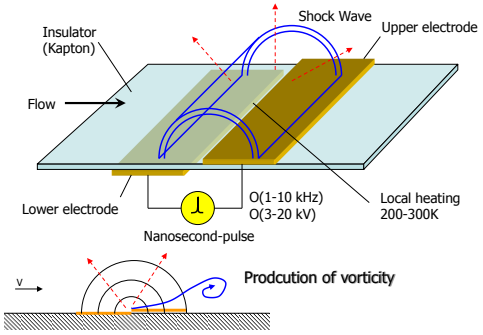

b) NPDBD actuator

Fig. 5 Working principle of Standard DBD (a) and Nano-pulsed DBD (b) actuator. The SDBD actuator produces a body force, F_b, whereas the Nano-pulsed actuator is based on thermal heating which leads to the production of shockwaves that in turn produce vortical structures.

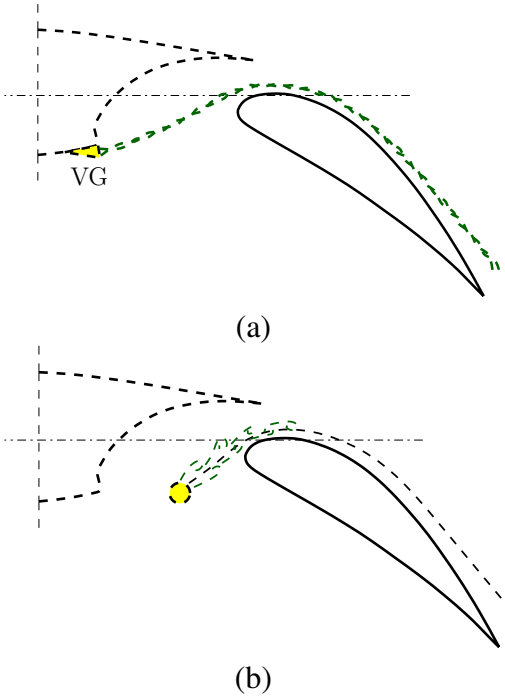

(a)

(b)

Fig. 6 Layout of the model with VG's applied on the main element lower surface (a) and a cylinder in front of the flap leading edge (b).

the cylinder may be stowed in the cove cavity. Ref. [27] has shown that the presence of such a cavity has no detrimental effect on the overall flap performance as the flow always separates at the sharp corner on the lower side of the slot.

3.2.3 Vortex generators

Based on the positive results that were obtained earlier with off-surface vortex generators (VG) [6], the lower side of the main element was equipped with VG's at the trailing edge. Again the flow separation control mechanism is based on increased mixing in the flap upper surface boundary layer (fig. 6a). The optimum VG position and dimension was determined in earlier test campaigns on a simplified wing-flap model.

3.2.4 Drooped spoiler

To improve the high lift characteristics new spoiler and flap kinematics are currently investigated in various research programs like Clean-Sky [8]. The so-called drooped spoiler panel was discussed by Reckzeh [11] and more recently by

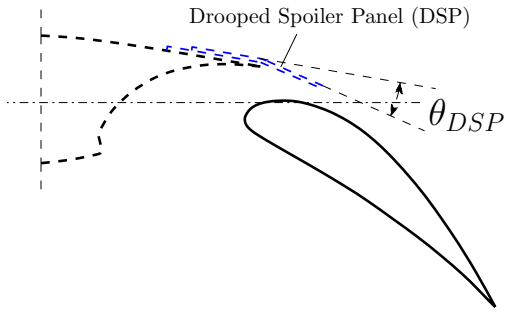

Fig. 7 Drooped spoiler panel (DSP) layout as applied in this research.

Wang and Wang[25].

In order to increase the low speed aerodynamic performance and reduce the complex flap kinematics and weight, the spoiler panel, which is directly positioned in front of the flap, is allowed to have a downward deflection for particular (high) flap deflections. In our study the drooped spoiler effect was simulated by adding a small additional panel at the main wing trailing edge. Its main purpose is the relieve of the large positive pressure gradient after the flap nose suction peak to prevent premature flow separation at large flap deflection angles (fig. 7).

3.3 Measurements

Balance measurements Since Model 1 was not equipped with pressure taps the overall model forces were determined using an external 6-component balance.

Pressure measurements Surface pressure measurements were performed were performed on Model 2 only. A total of 84 surface pressures were measured (56 on the main element and 28 on the flap). The wake of this model was measured using a dedicated wake rake that was positioned at approx. 1 m behind the model (fig. 4b). Moreover, at several stations the total pressure distribution in the wake and the boundary was determined by using a traversing a boundary layer probe.

Shadow graph technique (Schlieren Method) In case of the nano-pulsed plasma controller the flow in the vicinity of the actuator was visualized using the so-called Schlieren technique. This technique was essential in the detailed recognition of shock waves that were emitted from the actuator.

Surface flow visualization In addition to pressure measurements, tuft and flow visualization based on a fluorescent oil technique were carried out. These data were used to check the interpretation of the measured pressure data that were sometimes inconclusive with respect to the amount of separated flow over the surface. Because the tuft is extremely flexible, it will point in the direction of the flow.

4 Experimental results

4.1 Model 1

The flow control capabilities of nano-pulsed plasma actuators was first tested on a single element airfoil (Model 1)[5, 20]. The model was tested in wind speeds between $5\,m/s$ and $30\,m/s$ ($Re_c = 0.5 - 3.5 \times 10^5$). Earlier investigations indicated that the standard DBD actuators showed little effect at wind speeds beyond $V = 15\,m/s$ due to their limited momentum input. As the working principle of the NP-DBD actuator is quite different (the exact working principle is currently under investigation) significant effects were obtained for higher wind speeds. Fig. 8 shows the effect of an NP-DBD actuator applied on the nose of Model 1. In the stall regime a significant increase in the lift coefficient was obtained.

Although the exact working principle of the NP-DBD actuator is unclear to date the production of spanwise vortical structures is evidenced by the Schlieren images that were taken (fig. 9). The images clearly show the occurrence of vortices shortly after the pulse which in turn lead to flow reattachment. The vorticity production mechanism might either be the result of shock wave shear layer interaction or high speed heating (up to $T = 300\,K$). To get further insight in these mechanisms currently an additional re-

NACA63618 airfoil model with a double NP-DBD actuator applied close to the LE; Wind speed is$V = 30 m/s$.

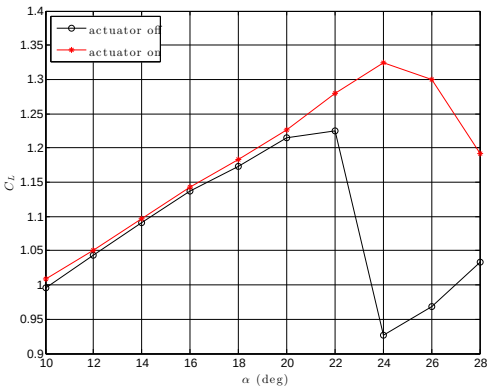

Fig. 8 Lift polar of Model 1 showing stall delay at high angle of attack. The angle of attack,α, was not corrected for windtunnel wall effects.

search program has been initiated at Delft University.

Furthermore, with these results in mind both the standard DBD actuator and the Nano-pulse actuator were tested on the flap of Model 2.

4.2 Model 2

4.2.1 Basic characteristics

To determine the reference characteristics for later application of flow control devices, first the optimal position of the flap with respect to the main element (the gap and overlap, fig. 10) was determined through a series of windtunnel tests.

Fig. 11 shows the effect of changing the gap for a fixed overlap of 8% in case of a flap deflection of $\delta_f = 15^o$. As long as the gap is well over 1% the effect of gap changes are relatively small. In case of a 1% gap the flow through the cove loses to much energy (total pressure) which results in a premature separation over the flap upper surface which in turn reduces the circulation over the airfoil.

An overview of gap and overlap effects for different flap settings is presented in figs. 11 and 12. As can be seen for a gap range of 2% to 4% and and overlap range of 0% to 1% of the chord, rather flat curves are obtained. Based on these data the gap and the overlap for the higher flap deflections (beyond $\delta_f = 40^o$ were selected 3% and 1% respectively. Typical pressure distributions for different angles of attack and a flap setting angle of $\delta_f = 50^o$, are presented in fig. 13.

It was found that for low angles of attack the flow over the flap is attached up to $\delta_f = 30^o$. However for larger flap deflections flap trailing edge flow separation starts to occur. The dent in the flap pressure distribution close to the nose (arrow in fig. 13) is the result of an interaction between the main element and the flap. It pushes the low pressure peak down to a lower level which in turn leads to a limited pressure rise behind the (2^{nd}) low pressure peak. This interaction between main element and flap is thus beneficial in the postponement of flow separation over the flap.

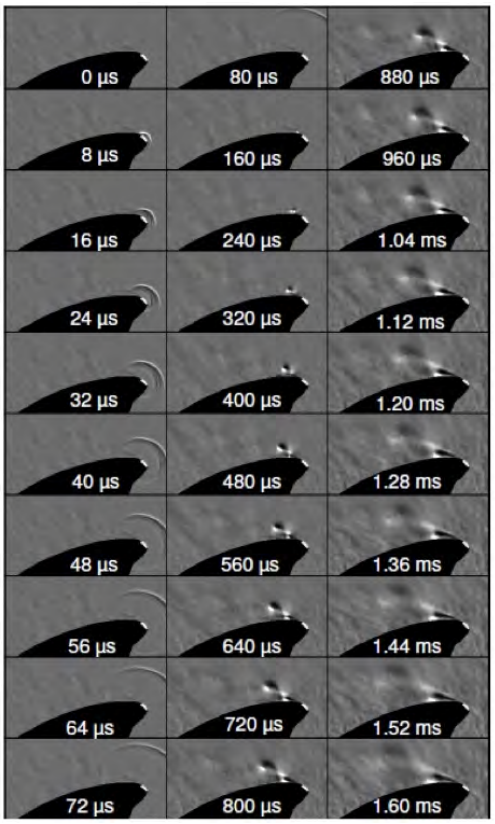

$\Delta t = 8\mu s, V = 30m/s, \alpha = 26^o, Re = 4 \times 10^5$

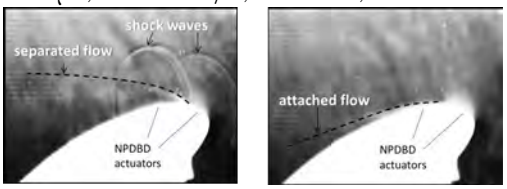

Actuation phase at time t_0 (left) and flow reattachment phase at (right) ; Carrier frequency $f_c = 200Hz, V = 30m/s, \alpha = 26^0$.

Fig. 9 Schlieren images taken over Model 1, showing the presence of Nano-plasma actuator induced shock waves with subsequent vortical structures and flow reattachment.

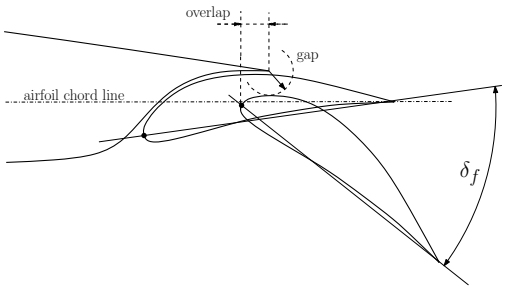

Fig. 10 Definition of gap and overlap for the X400 wing-flap model.

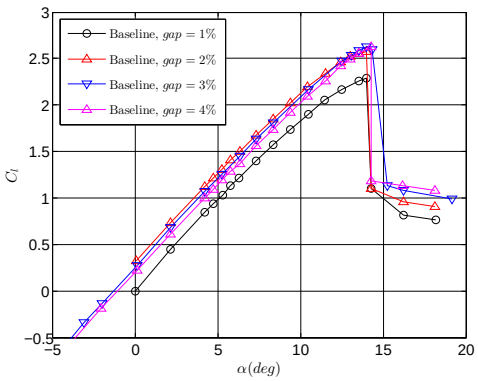

Fig. 11 Effect of the gap on the lift polar for $\delta_f = 15^o$ and an overlap of 8%.

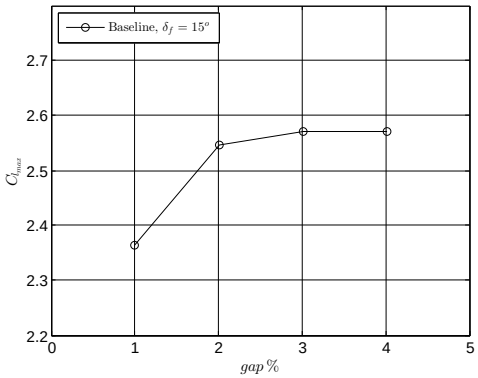

(a) $\delta_f = 15^o$; $overlap = 8\%$; $Re = 2.0 \times 10^6$

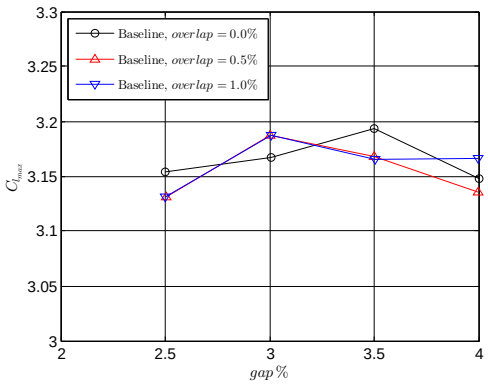

(b) $\delta_f = 30^o$; $Re = 1.7 \times 10^6$

Fig. 12 Overview of gap and overlap effect on maximum lift coefficient.

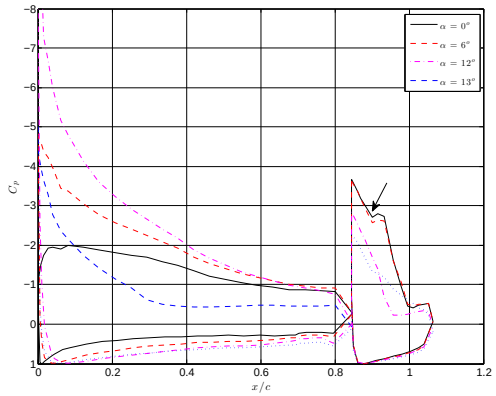

Fig. 13 Typical pressure distributions over the baseline configuration with large flap deflection; $Re = 1.7 \times 10^6$; $\delta_f = 50^o$.

4.2.2 Effect of lower side vortex generators

Model 2 was tested at a constant wind speed of $V = 50m/s$ ($Re_c = 2 \times 10^6$). To prevent laminar separation bubbles zigzag type transition strips were applied at appropriate position at the wing lower side. The vortex generator consisted of Delta-type skewed elements as presented in fig. 14.

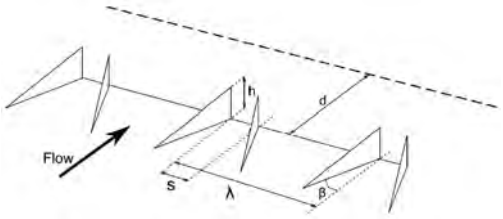

Fig. 14 Vortex generator geometrical definitions.

For this research only the counter rotating VG's were be tested at several sizes height. The geometrical definitions of the VG's, include:

- λ the mutual spacing of the vortex generators
- h, the height of the vortex generator
- d, for the distance between the VG's and the bottom trailing edge of the Model 2.

The vortex generators are all tested for different values for these parameters. Based on this fixed values were chosen of $\beta = 18^o$ and and $s = h$ respectively, for which Veldhuis and van der Steen [6] found best results on a simplified windtunnel model.

Fig. 15 shows the lift performance of two sets of multiple VG configurations. It can be seen from the figures that the VG configurations all show an increase in lift at lower angles of attack but generally have a decrease in lift near the stall angle. However, it should be noted that in our case the main area of interest is the flow separation control at low α and not at $C_{l_{max}}$. This is because the model is tested with a trailing edge flap only which lacks a leading edge slat that gives a better performance at higher angle of attack.

From fig. 15 it can be seen that VG's with smaller and larger heights ($h^* = 0.010$ and $h^* = 0.070$) show only minor effect in lift improvements. In this case the VG height is made dimensionless with the wing chord (600mm), $h^* = h/c$. The smaller height, $h^* = 0.010$, results in too small vortices that are insufficient of mixing enough high energy flow to the boundary layer at the flap. The larger VG's, $h^* = 0.070$, are probably causing adverse vortex interaction since they lead to very fluctuating lift values also visible in the lift polar. The spacing shows an effect where values should neither be too large nor too small for an optimal vortex performance. VG's at a spacing of $\lambda/h = 6.5$ and $\lambda/h = 4.5$ do not result in a significant lift improvement. This is probably due to a too large spacing where an insufficient amount of healthy air is pumped into the boundary layer.

Only the VG configuration with spacing $\lambda/h = 4.0$ and height $h^* = 0.023$ shows a significant performance gain over the whole range of α, this setup is found to be the optimum VG configuration. In this case a gain of $\Delta C_l = 0.11$ is found at $\alpha = 0^o$,which is an improvement of 6% compared to the baseline. At high angles improvements are obtained of $\Delta C_{l_{max}} = 0.064$ an improvement of 2.2%. It is clear for all configurations that stall is not delayed. This is not surprising since the stall for this airfoil flap model is mainly determined by the main element stall characteristics and not the performance of the flap.

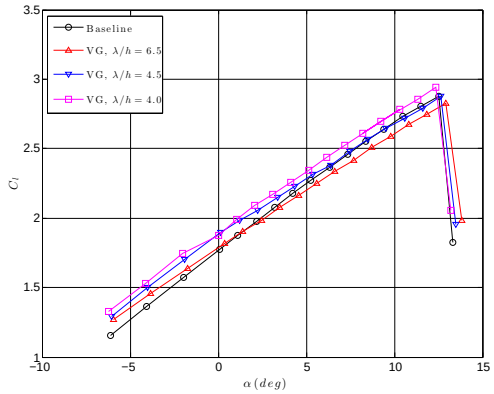

Set 1, $h^* = 0.023$, $d^* = 0$

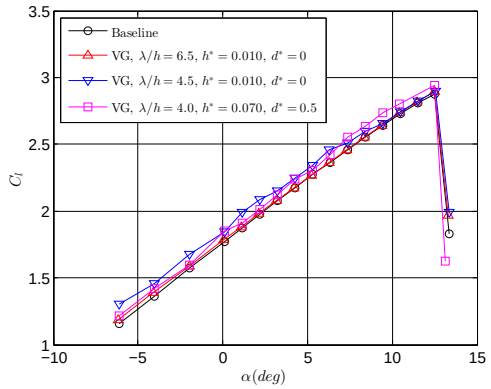

Set 2

Fig. 15 Effect of height, spacing and edge distance on the lift polars for multiple VG configurations at $\delta_f = 55^o$

4.2.3 Effects of cylinders

Although the effect of cylinder was tested for different flap angles, only the results for $\delta_f = 55^o$ will discussed here. Fig. 17 shows the effect of on the lift performance of several cylinder configurations. It can be seen that multiple cylinder configurations show significant improvement over the complete α-range. Cylinders with varying diameters all show a performance gain when positioned properly, in the range of $r^* = 0.06 - 0.09$ and $\theta = 30^o - 37^o$ (fig. 16). Here r^* and θ respectively denote the distance from a reference point and angle with respect to the horizontal. The positioning seems to be more important for the lift improvement than the particular cylinder diameter.

The cylinder performs best with diameter $D^* = 0.0167$, but hardly loses efficiency for larger diameters. The optimum configuration is

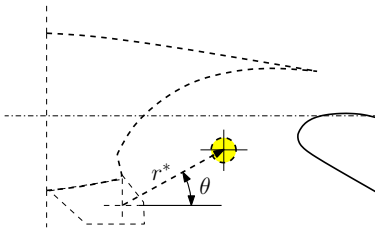

Fig. 16 Definition of cylinder position parameters.

found for $D^* = 0.0167$, $r^* = 0.090$ and $\theta = 37^o$ The optimum cylinder diameter of $D^* = 0.0167$ corresponds to a reduced frequency of $F^+ = 3.6$. For this configuration the largest gain in lift is found near $\alpha = 0^o$ where lift increases up to $\Delta C_l = 0.32$. This is an astonishing improvement of 18% compared to the baseline. At high angles improvements are obtained of $\Delta C_{l_{max}} = 0.24$. Similar to the case of the vortex generators the cylinders do not delay the stall of the airfoil flap model.

Fig. 18 shows the pressure distribution for the optimum cylinder configuration compared to the baseline model at $\alpha = 0^o$ and 12^o. It shows at both angles of attack that the low pressure peak at the leading edge of the upper flap surface is significantly lower with the cylinder installed. The pressure rise is also found further towards the flap trailing edge, which suggests that flow separation is postponed. It further seems that the pressure recovery is smoother for the cylinder configuration. The enhanced flap lift reduces pressures at the upper airfoil which is achieved through an increased circulation effect of the flap on the main element. It should be noted that apparently a small downstream displacement of the separation point may lead to noticeable effects on the overall lift of the model.

Fig. 19 shows fluorescent oil visualization pictures of the flap for the baseline and cylinder configuration at $\alpha = 0^o$ and $\alpha = 10^o$ respectively. Observation of fig.19a shows that the fluorescent oil is streaked downstream (from right to left) up till the dividing vertical line. This is the point where laminar to turbulent transition takes place. At this point, inside the bubble, there is a very low flow speed and oil is clumped up resulting in

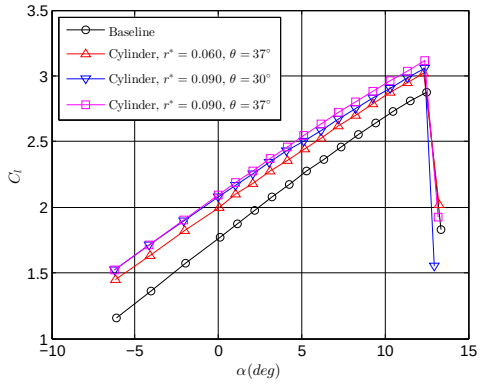

(a) Cylinders set 1, $D^* = 0.0167$

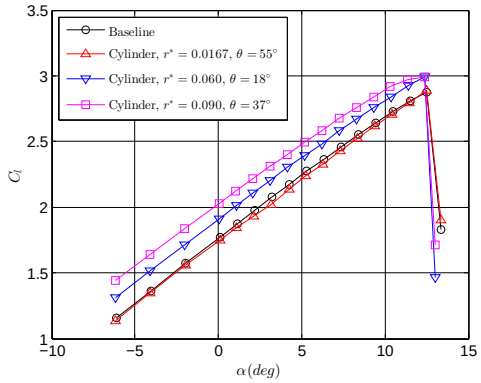

(b) Cylinders set 2

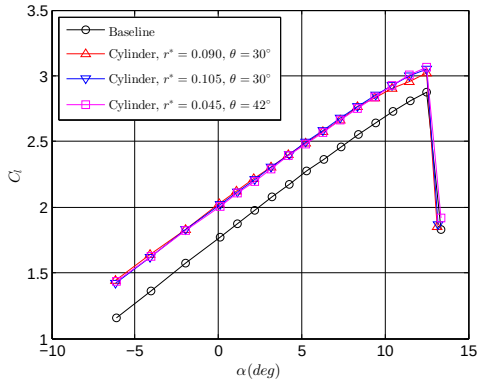

(c) Cylinders set 3, $D^* = 0.025$

Fig. 17 Effect of size and positioning on the lift for different cylinder configurations at $\delta_f = 55^o$.

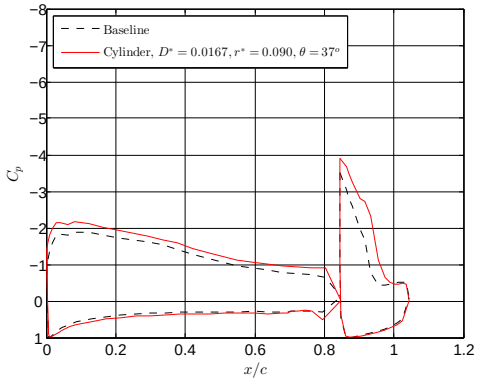

(a) $\alpha = 0^o$

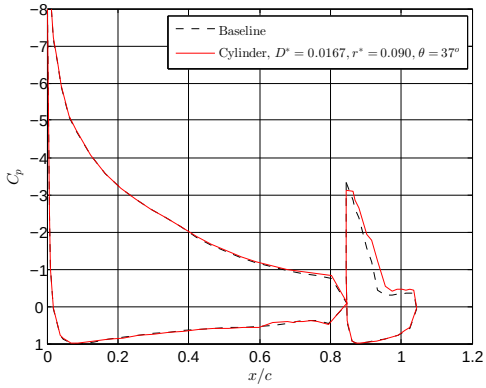

(a) $\alpha = 12^o$

Fig. 18 Pressure distributions for optimum cylinder and baseline configuration at low and high α; $D^* = 0.0167$, $r^* = 0.090$, $\theta = 37^o$, $\delta_f = 55^o$.

the clear dividing line. After the bubble the flow reattaches and becomes turbulent. In this area all the oil moves downstream leaving a rather clean surface. Further downstream the turbulent flow is unable to cope with the adverse pressure gradient and separates. The separation point is clearly seen by a second dividing line where the flow has come to rest. After this point the flow is non-uniform and circulates and oil is smeared in different directions.

These oil flow patterns are seen in all the pictures, although clear differences are also visible. Most noticeable is the clear shift downstream of the second vertical line for the cylinder configuration model with respect to the baseline configuration. This confirms the observations from the pressure distributions that flow separation has been postponed. Again this proves that the cylinder vortices indeed have a positive effect on delaying flow separation. Comparing the oil patterns between the baseline and cylinder configurations also shows that the flap with the cylinder in front exhibits a turbulent layer directly from the leading edge. Hence no laminar separation bubble is present in this case.

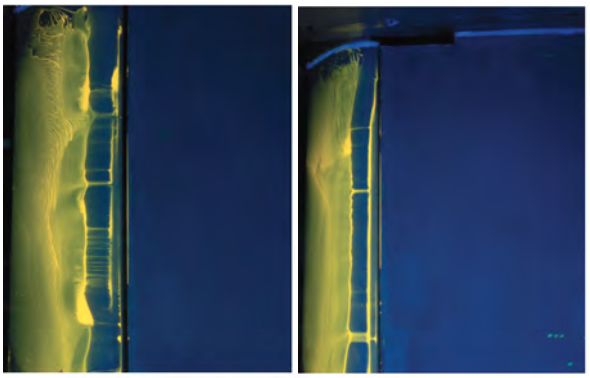

Baseline, $\alpha = 0^o$(left), $\alpha = 10^o$(right)

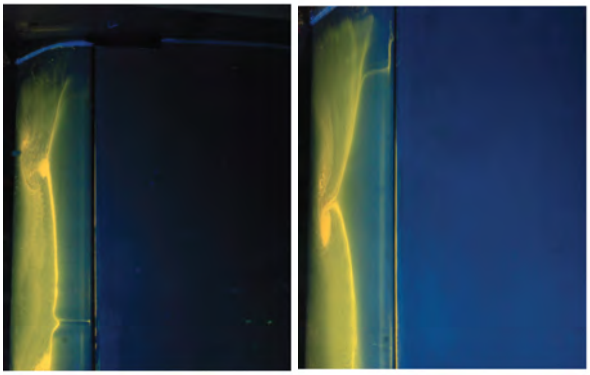

Cylinders, $\alpha = 0^o$(left), $\alpha = 10^o$(right)

Fig. 19 Oil flow visualization on the flap for the baseline and optimum cylinder configuration at $\delta_f = 55^o$. The main flow direction is from the right.

4.2.4 Plasma actuators

Standard plasma actuator To control the flow over the flap both standard DBD and NP-DBD actuator were utilized (fig. 20). The AC DBD actuator consist of $60\mu m$ thin rectangular copper electrodes made out of self-adhesive copper tape. A dielectric layer (Kapton) separates the upper electrode from the lower one. Tests are carried out with one to three Kapton tape layers. To prevent the actuators discharging with the model itself, the surface is locally insulated by one Kapton layer before placing the actuator. The thickness of one such layer measures $2mil$ ($1mil = 25.4\mu m$). The upper electrode is connected to the HV output cable of a *TREK 20/20C HV* amplifier (± 20kV, ± 20mA, 1000W) while the lower electrode is connected to a grounded cable.

Separate measurements in which the length of surface roughness was changed over the span

Fig. 20 Standard DBD actuator positioned close to the LE of the flap. At the dark rectangular area multiple layers of dielectric were placed to prevent discharge with the metal orifice.

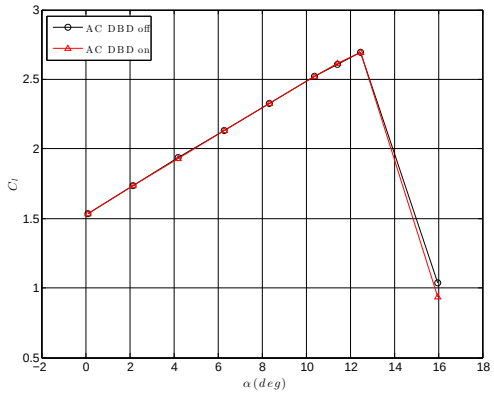

Fig. 21 Effects of the standard (AC) DBD plasma actuator placed on the LE flap on the lift polar; $\delta_f = 45^o$, $Re = 1.7 \times 10^6$; width upper electrode $w_u = 10mm$; applied voltage $V = 28kV_{pp}$; carrier frequency $f_ac = 700\,Hz$

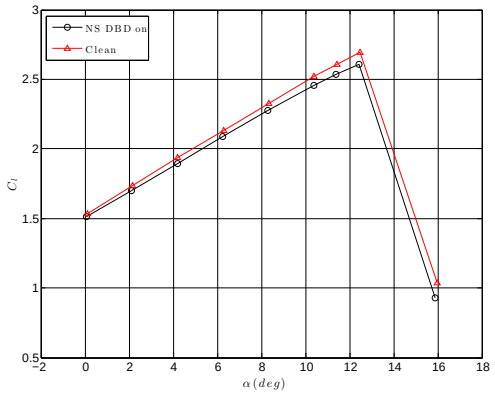

Fig. 22 Typical example of the effect of the NS DBD plasma actuator placed on the LE flap on the lift polar. ; $\delta_f = 45^o$, $Re = 1.7 \times 10^6$, carrier frequency $f_ac = 700\,Hz$, burst frequency $f_b = 3.3kHz$.

showed that an actuator should span at least 80% of the total flap span to obtain reasonable quasi-2D effects. A longer actuator length would lead to limited power input per meter resulting in reduced effects on the flow.

The range of parameters that were changed during the experiments include

- actuator length $20-100cm$
- applied voltage $20-30kV$
- carrier frequency $600-800Hz$
- actuator position w.r.t. separation line
- tunnel speed $10-40m/s$

The possible effects in these experiments were first quantified by applying tufts visualization on the flap's upper surface. As more or less expected, in none of these cases AC DBD plasma actuator succeeded in showing any separation postponement effects during the tuft visualization. Even not at very low velocities up to 10m/s. This can be seen in fig. 21 where the lift polar is presented for the actuator on and off test.

Nano-pulsed actuator Following a similar approach as for the AC actuator the NP-DBD actuator was also tested for different configurations while maintaining the proposed minimum actuator length and the energy discharge density. The actuators were all driven by the maximum voltage the generator can deliver i.e. $10kV$. First, the effect of the actuator is investigated using tuft visualization by varying the following parameters:

- actuator length $20-100cm$
- actuator position w.r.t. separation line
- tunnel speed $10-40m/s$

Since no visible change in the separation line location on the flap could be observed, the amount of parameters to investigate were limited. Fig. 22 compares the actuator-on case with the clean case (actuator completely removed). This is a typical result obtained for most of the NP DBD actuators in this research. The lift coefficient is lower in the case of the active actuator. Apparently the flow situation for the single element airfoil in section 4.1 is quite different here and no beneficial effect of the actuator is noticed. Furthermore, the somewhat lower value of the lift coefficient compared to the clean case is very likely a result of the thickening effect of due to the actuator itself which leads to earlier flow separation.

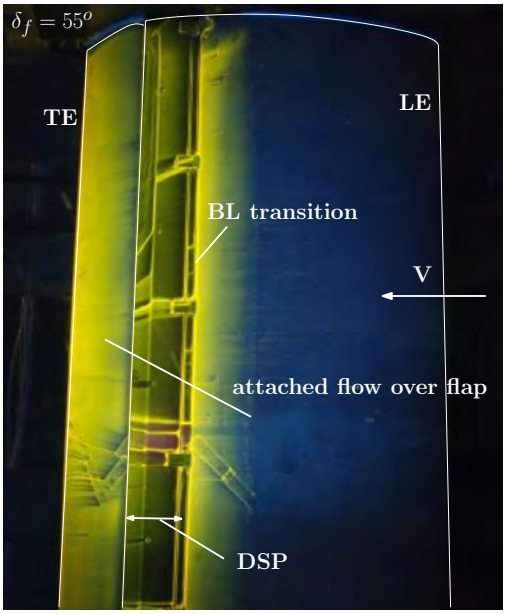

Fig. 23 Flow visualization over the upper surface of Model 2, indicating fully attached flow over the flap when the DSP is applied; $\alpha = 0^o$, $\delta_f = 55^o$.

4.2.5 Drooped spoiler

The drooped spoiler (DSP) was investigated at a flap angle of $\delta_f = 55^o$ since the main goal of its application was to reattach the flow in the area of a large adverse pressure gradient. The expected effect is an increased effective camber of the airfoil with associated increase in the lift coefficient. Before taking pressure data surface flow over the model was checked using the fluorescent oil technique. Fig. 23 indicates that the DSP with a length of approximately 30*mm* (5% chord) and a deflection angle of $\theta_{DSP} = 15^o$ now leads to a fully attached flow. This is a considerable improvement over the other techniques that only led to a limited delay of flap stall.

However, when looking at the lift polar of Model 2 equipped with DSP (fig. 24) a disappointing effect is noticed. For small angles of attack the lift has increased slightly but beyond $\alpha = 4^o$ the value drops considerably below the baseline result. Although the flow is fully attached over the full angle of attack range and the flap introduces a stronger downwash directly behind its trailing edge, the adverse pressure gradient is now so strong that "wake bursting" occurs.

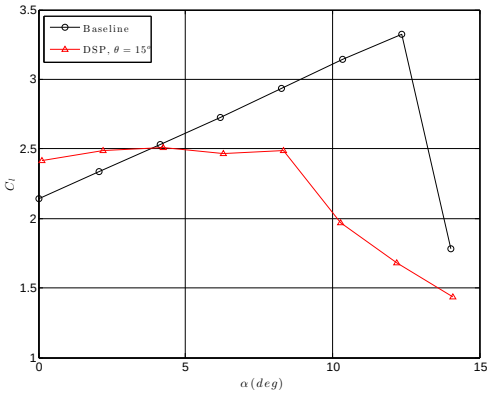

Fig. 24 Comparison of the lift polar of the baseline model and the model equipped with DSP ($\theta_{DSP} = 15^o$).

This phenomenon, that received only limited attention in literature, is not very well understood so-far. The overall circulation around the model is considerably reduced due to the wide wake in which flow reversal takes place. To understand the behaviour of the model equipped with DSP the pressure distributions for $\alpha = 0^o$ and 8^o are considered in fig. 25.

The higher lift due to the DSP at low angles of attack (fig. 25a) seems to be a direct result of the forced flow attachment (see flap TE) that leads to increased circulation on the main wing. In this case the boundary layer thickness on the wing upper side combined with the moderate positive pressure gradient does not yet lead to significant wake bursting. However, the situation changes completely for the larger angle of attack (fig. 25b). The DSP again forced fully attached flow over the flap but the thicker upper side boundary layer over the model now leads to a strong wake bursting effect. The lift on both the main wing element and the flap is much lower than found for the baseline configuration.

Wake bursting is associated with flow reversal in the wake (of the main element) and as such is hard to detect through surface pressure measurements and surface flow visualization. Flow reversal was indeed noticed in our experiment by scanning the flow field behind the model with DSP using a Pitot tube (fig. 26).

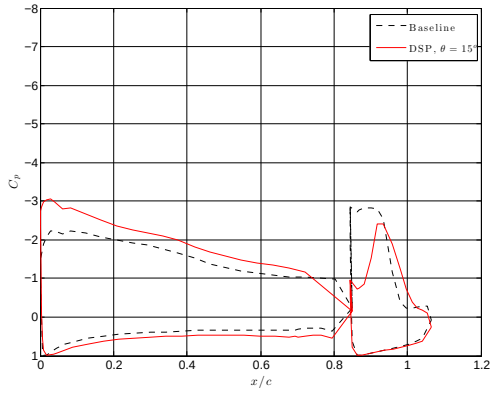

a) $\alpha = 0^o$

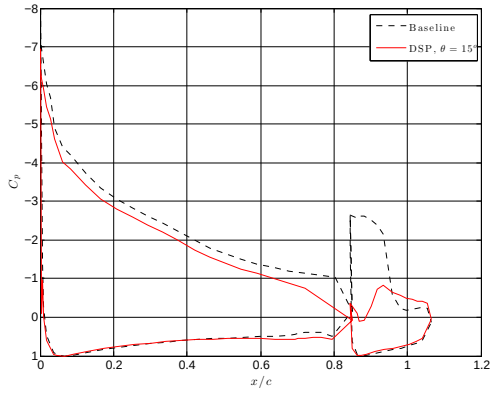

b) $\alpha = 8^o$

Fig. 25 Pressure distributions of the model equipped with DSP ($\theta_{DSP} = 15^o$) for $\alpha = 0^o$ and 8^o.

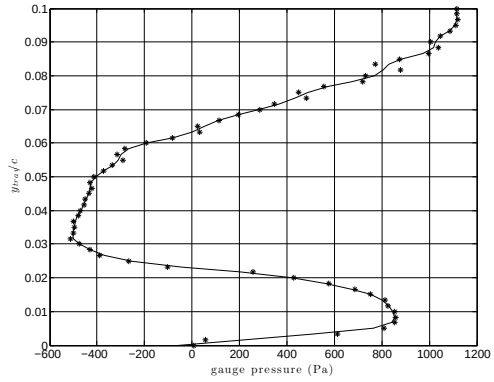

Fig. 26 Wake traverse result of a Pitot tube at short distance behind the model showing off-surface flow reversal, in the range $y_{trav}/c = 0.022 - 0.062$, indicating the presence of "wake bursting"; $\alpha = 8^o$.

With the wake bursting occurring as a result of the very powerful flow control effect of the DSP one might argue that apparently passive methods for the increase of maximum lift for this particular model are quickly exhausted. This also suggests that any active/passive flow separation control method for flaps in a high lift system might have limited applicability when strong pressure gradients exist in the wake flow area.

5 Conclusions

Experimental analysis of several passive and active control techniques to control flow separation over a highly deflected flap have been performed successfully. Among the techniques that were used are: VG's on the main element lower surface, cylinder in front of the flap leading edge, plasma actuators close to the wing leading edge and a drooped spoiler panel. From the experimental results the following main conclusions can be drawn.

- The application of NPDBD actuators showed significant suppression of flow separation over a single element airfoil at speeds up to 30-40 m/s. However, the effects of both SDBD and NPDBD actuators on the flap of a multi-element airfoil were negligible. The mechanism by which the NPDBD actuator suppresses flow separation under certain circumstances is still unclear.

- The application of VG's on the wing lower side as well as a cylinder in front of the flap, leads to a noticeable increase of the lift at flap deflections were serious trailing edge separation occurs. The working principle of these passive techniques is based on enhancement of increased mixing in the flap boundary layer due to either streamwise vortices (VG's) or lateral oriented vortices produced by the cylinder.

- A drooped spoiler panel (DSP) positioned at the back of the main wing (simulating a downward deflected spoiler) led to a

fully attached flow over the flap at flap angles up to $\delta_f = 55^o$. However, for moderate to high angles of attack the wake of the main element experiences a very large positive pressure gradient which leads to wake bursting. The occurrence of this phenomenon very likely limits the positive effect of passive and active flow control at the flap of multi-element airfoils.

References

[1] Gad-el Hak, M. Flow Control; Passive, Active, and Reactive Flow Management. Cambridge University Press, 2000.

[2] Gilarranz, J., Traub, L. and Rediniotis, O, Characterization of a Compact, High-Power Synthetic Jet Actuator for Flow Separation Control. 40th AIAA Aerospace Sciences Meeting and Exhibit, 14-17 January 2002. AIAA 2002-0127.

[3] Greenblatt, D. and Wygnanski, I., The control of flow separation by periodic excitation. Progress in Aerospace Sciences, 36:487-545, 2000.

[4] M. Bauer, I. Peltzer, W. Nitsche and B. Gölling, Active flow control on an industry-relevant civil aircraft half model, Notes on Numerical Fluid Mechanics and Multidisciplinary Design, 2010, Volume 108/2010, 95-107, DOI: 10.1007/978-3-642-11735-0_7

[5] Correale, G., Popov, I., Ratikin, A., Starikovskii, A. and Veldhuis, L.L.M., Flow Separation Control on Airfoil with Pulsed Nanosecond Discharge Actuator, 63rd Annual Gaseous Electronics Conference and the 7th International Conference on Reactive Plasmas, Vol. 55, Number 7.

[6] Veldhuis, L.L.M. and van der Steen, M., Flow separation control by off surface elements, AIAA-2010-4684, 28th AIAA Applied Aerodynamics Conference, Chicago, Illinois, June 28-1, 2010

[7] Boermans, L.M.M. and Rutten, P.B., Two-dimensional aerodynamic characteristics of airfoil NLF-MOD22 with fowler flap, Internal Report LSW-95-3, Delft University of Technology, 1995

[8] Cleansky, http://www.cleansky.eu

[9] Smith, A.M.O., High lift aerodynamics, Journal of Aircraft, Vol. 12, No. 6, 1975

[10] van Dam, C.P., The aerodynamic design of multi-element high-lift systems for transport airplanes, Progress in Aerospace Sciences 38 (2002) 101–144

[11] Reckzeh, D., The Role of High-Lift Aerodynamics . KATnet II conference (pp. 1-18). Bremen: Airbus, 2009

[12] Göksel, B. , D. Greenblatt, D., Rechenberg, I., Singh, Y, Nayeri, C.N. and Paschereit, C.O., Pulsed Plasma Actuators for Separation Flow Control B, Conference on Turbulence and Interactions TI2006, May 29 – June 2, 2006, Porquerolles, France

[13] Roth, J.R. Physics and phenomenology of plasma actuators for control of aeronautical flows. s.l. : J., Phys. D:Appl. Phys. 40, 2010.

[14] Post, M. L. and Corke, T.C. Separation control on high angle of attack airfoil using plasma actuators. s.l. : AIAA Journal, vol. 42, no11, pp. 2177-2184, 2004.

[15] Post, M.L. and Corke, T.C. Separation control using plasma actuators: dynamic stall vortex control on oscillating airfoil. s.l. : AIAA Jornal, 44 3125, 2006

[16] Enloe, et al. Mechanisms and Responses of a Single Dielectric Barrier Plasma Actuator: Plasma Morphology. AIAA Journal, v. 42, n. 3 : s.n., 2004. pp. pp. 589-594.

[17] Kotsonis, M. , Dielectric Barrier Discharge Actuators for Flow Control, PhD dissertation, Delft University of Technology, 2012

[18] Kotsonis, M., Ghaemi, S., Veldhuis, L., & Scarano, F., Measurement of the body force field of plasma actuators. Journal of Physics D: Applied Physics, 44(4), 2011.

[19] Kotsonis, M. and Veldhuis, L., Experimental study on dielectric barrier discharge actuators operating in pulse mode, J. Appl. Phys. 108, 113304, 2010.

[20] Correale, G., Popov I., Rakitin A., Starikovskii A., Hulshoff, S. ,Veldhuis L., Flow Separation Control on Airfoil With Pulsed Nanosecond Discharge Actuator, AIAA-2011-1079 49th AIAA Aerospace Sciences Meeting, Orlando, Florida, Jan. 4-7, 2011.

[21] Moreau, E. Airflow control by non-thermal plasma actuators. s.l. : J. Phys. D: Appl. Phys. 40 605, 2007.

[22] Okita Y, Jukes T N, Choi K-S and Nakamura K. Flow reattachment over an airfoil using surface plasma actuator. s.l. : AIAA 2008-4203, 2008, 2008.

[23] Starikovskii, A.Y. Nikipelov, A.A., Nudnova, M.M.M and Roupassov, D.V. SDBD plasma actuator with nanosecond pulse-periodic discharge. s.l. : Plasma Sources Sci. Technol. 18.

[24] Little, J., Takashima, K., Nishihara, M. , Adamovich, I andSamimy, M. High Lift Airfoil Leading Edge Separation Control with Nanosecond Pulse Driven DBD Plasma Actuators. s.l. : AIAA 2010-4256, 2010.

[25] Xiao-liang Wang and Fu-xin Wang, Aerodynamic Characteristics of High-Lift Devices with Downward Deflection of Spoiler, Journal oif Aircraft Vol. 48, No. 2, March–April 2011

[26] Nishri, B. and Wygnanski, I., " Effects of periodic excitation on turbulent flow separation on a flap. AIAA Journal, 36(4):547-556, April 1998

[27] Potter, R.C. and van Dam, C.P., Viscous flow analysis of a subsonic transport aircraft high-lift system and correlation with flight data, NASA-CR-199610, 1995

Copyright Statement